Experimental Study on the Drag Forces on a Twin-tube Submerged Floating Tunnel Segment Model in Current

Shi Deng[a], Haojie Ren[b], Yuwang Xu[b *], Shixiao Fu[a, b, c], Torgeir Moan[a, c,d], Zhen Gao[a, c,d]

[a] Department of Marine Technology, NTNU, NO-7491 Trondheim, Norway

[b] State Key Laboratory of Ocean Engineering, Shanghai Jiao Tong University Shanghai, 200030 China

[c] Centre for Ships and Ocean Structures, NTNU, Marine Technology Centre, NO-7491, Trondheim, Norway

[d] Center for Autonomous Operations and System, NTNU, , Marine Technology Centre, NO-7491, Trondheim, Norway

Abstract

In this paper, the drag forces on a rigid segment of a twin-tube submerged floating tunnel (SFT) under various Re number and submergence are experimentally investigated with a simplified rigidly connected tandem twin-cylinder model towed in a tank. The effects of the spacing distance between two cylinders and vortex-induced vibration (VIV) on the drag forces are investigated through stationary and self-oscillation towing tests. It was found that, in the stationary cases, the drag forces on the cylinders act in opposing directions when the spacing ratio is 2 and 3, which leads them attracting each other. Under VIV conditions, the drag forces are significantly amplified, namely that, the maximum mean drag coefficients of the up- and downstream cylinders increase from 1.27 to 4.1 and 0.43 to 1.7, respectively. As for the submergence effect, it was found that both the VIV response amplitude and mean drag coefficient decrease with the decreasing of the submerged depth, especially when the depth ratio is below 3.7.

Keywords:
Submerged Floating Tunnel, Drag Force, Spacing Distance, Vortex Induced Vibration, Submergence

1. Introduction

The Norwegian Public Road Administration (NPRA) is planning to upgrade Coastal Highway E39, which is located on the west coast of Norway, by replacing the ferry connections with a submerged floating tunnel (SFT). The SFT consists of two rigidly connected identical concrete tunnel tubes with a diameter of 12.6 m in a tandem configuration. It is suspended 24.6-32.6 m below the water surface, which is defined as the distance from the lower side of the tunnel tube to the initial free surface, as shown in Fig. 1 [1]. In this submerged depth, current load is a key factor challenging the reliability and fatigue lifetime. The hydrodynamic force acting on the tunnel in a current

*Corresponding author: Yuwang Xu; E-mail: xuyuwang@sjtu.edu.cn

field consists of the lift force in the crossflow (CF) direction and the drag force in the inline (IL) direction. The former one will excite small amplitude but high frequency oscillation in the CF direction, namely vortex-induced vibration (VIV) which has been found to significantly amplify the drag forces [2]. The mean drag force causes steady deformation of the tunnel tube with a relatively large amplitude which subsequently affects the structural strength [3-6]. The Morison equation is typically used to calculate the mean drag force on the tunnel tube during its strength and safety design. Mean drag force coefficients of the two tunnel tubes are different from those of the conventional single cylinder system, and heavily depend on the spacing distance since it is a key parameter to decide the flow pattern between and behind the tandem twin cylinders [7]. Free surface could also affect the mean drag coefficients of the SFT because of its small submerged depth [8]. Thus, investigations of the effects from VIV, spacing ratios (defined by the ratio between center-to-center distance dividing the cylinder diameter) and submergences on the mean drag forces of SFT are necessary [8-12].

Many researchers have performed physical model tests with a single cylinder. As for the drag amplification due to VIV [13, 14], the results from previous studies show that the mean drag coefficient synchronizes with the VIV response amplitude [13-16], and the maximum values coincidently appear at the same time [17]. In addition, Khalak and Williamson presented the influences of system parameters, such as the mass and damping ratio, on the VIV-amplified drag forces [17, 18]. In the study of the effects of submergence, most of the researchers are focused on a fixed cylinder [19-21]. The modal tests and numerical simulations have shown that the free surface can limit the vortex formation as the cylinder approaches it. Meanwhile, the VIV response amplitude and mean drag force decreases monotonically as the immersion depth decreases [9, 12]. The effect of the submergence on VIV is normally discussed with respect to the Froude number $\left(F_r = \frac{U}{\sqrt{gh}}\right)$, which is defined by the flow velocity U, gravitational acceleration g and submerged water depth h [13]. The previous studies have led to a comprehensive understanding of the features and mechanisms of VIV-generated drag amplification and the effect of the submergence for a single-cylinder.

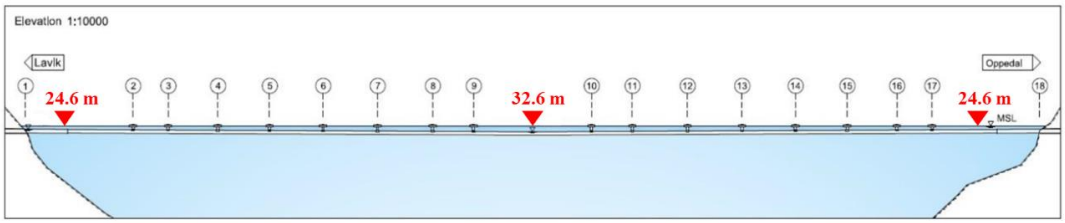

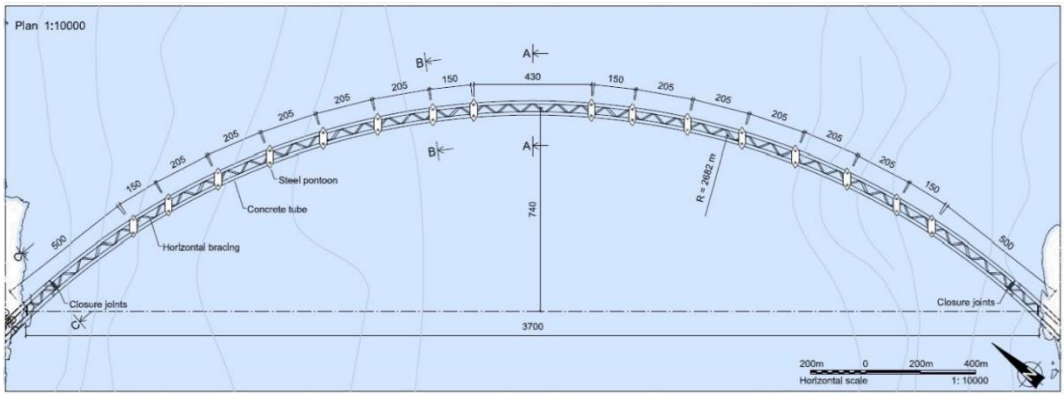

Fig. 1 SFT configuration [1]

However, the floating tunnel convinced by NPRA is composed of two identical tubes that are rigidly connected in tandem through truss structures [1]. For the tandem twin cylinders structure, some researchers have studied the effect of the center-to-center distance on the drag forces on the up- and downstream cylinders separately at low Reynolds number (Re) under static condition through towing tests or numerical simulations [3, 22-24]. It was observed that the drag coefficients of the two stationary cylinders gradually increased with the increases of the spacing ratio. A critical spacing ratio ($\lambda = 4.0$) has been found, which corresponds to the point where an abrupt increase appears in the drag coefficient [22], and the drag coefficient of the upstream cylinder approaches to that of the single cylinder [22, 25, 26]. Compared with an isolated cylinder, a large amplitude of oscillation and a wider lock-in region are found for cylinders in tandem arrangement [27]. The synchronization curve for the upstream cylinder is similar to that of an isolated cylinder, but it displays a shift on the reduced velocity axis depending on the spacing ratio [28, 29]. Meanwhile, for the downstream cylinder, it is found that the VIV amplitude, frequency and amplified drag forces are highly affected by its own reduced velocity as well as that of the upstream cylinder[30, 31].

However, those previous studies on drag forces of twin cylinders in tandem arrangement were based on either stationary model tests with large submergence, or unconnected (two cylinders oscillate individually) cylinders which are not suitable for the design of SFT which comprising two rigidly connected tubes. The VIV-generated drag amplification and the free surface effect on oscillating rigidly connected twin cylinders are still unclear and require further research.

In this study, a series of stationary model towing tests and self-oscillation experiments were conducted to investigate the effect of the spacing distance, VIV and submergence on the drag forces acting on rigidly connected tandem twin cylinders. The reliability of the experimental setup was first validated by comparing the experimental results of a stationary single cylinder in steady flow with the published data in the literature. Then, the effect of the spacing distance, VIV and submergence on the drag forces on the tandem twin-cylinder model was investigated.

2. Experimental Setup

2.1 Test Setup

In the study of VIV of flexible cylinders, such as the submerged floating tunnel and marine risers, there are normally two approaches. The first one is using a rigid segment model. It can provide a basic understanding of the VIV features, especially the hydrodynamic forces [18, 32]. The second one is to use a long and flexible cylinder model, mainly focusing on its deformations [16, 33]. In the second approach, the scaling from the prototype to the experimental model is more challenging because many parameters, such as the mass, length, diameter, stiffness and so on, should be considered. In the first approach, as applied in the paper, we mainly guarantee two parameters, i.e., mass ratio and reduced velocity, to be similar between the experimental model and the prototype, which are the key parameters that determine the oscillation amplitude and hydrodynamic forces.

The experiments were conducted in the Marine Cybernetics Laboratory towing tank at the Norwegian University of Science and Technology; the dimensions of the tank are 40 m × 6.45 m ×1.5 m. The maximum speed of the towing carriage is 1.2 m/s. The test setup consists of a towing carriage, two support frames and a rigidly connected tandem twin-cylinder model. The two smooth rigid cylinders are made of aluminum with a relative surface roughness $k/D = 0.6 \times 10^{-5}$ (k is the average height of the surface irregularities and D is the cylinder diameter). The diameter and length of the cylinder are 0.1 m and 2.05 m, respectively. The cylinder models were elastically mounted between two support frames that were suspended beneath a towing carriage, as shown in Fig. 2 and 3. Two groups of springs were equipped on the support frame to provide the restoring forces for the models. In the self-oscillation test, the model is only allowed to oscillate vertically, i.e. in the CF direction. A pair of low-friction tracks was mounted on one side of each frame to guide the CF motion. One displacement sensor and two force sensors were set up at both ends of the cylinder. The drag forces acting on each cylinder and the CF displacement response were measured simultaneously and recorded in digital form.

Two methods were adopted to avoid 3D effects stemming from the finite length of the cylinder. First, two dummy cylinders with the same diameter as the model were assembled at both ends of the model. A small space (<1 mm) was left between the dummy cylinder and the model to guarantee that the force transducer measured only the force acting on the model. Second, two circular endplates were assembled outside the dummy cylinder to reduce the impact of the other devices on the flow field.

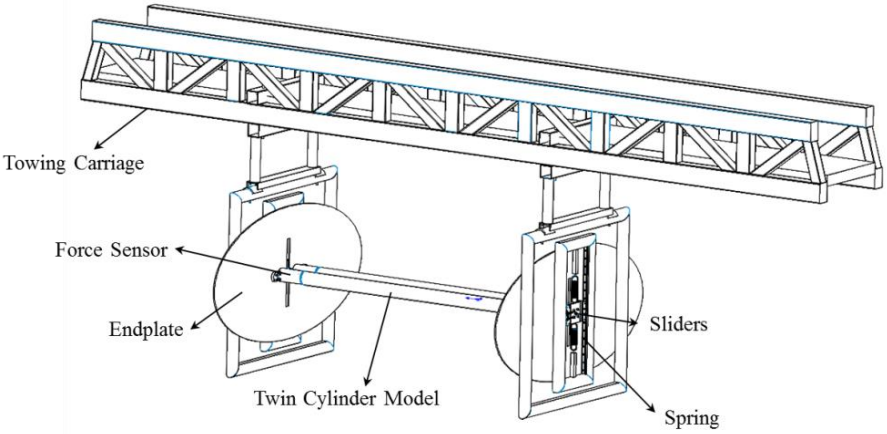

Fig. 2 Sketch of the experimental setup

Fig. 3 Photograph of the experimental setup

2.2 Test Arrangement

Fig. 4 shows the definition of the spacing ratio, which is equal to the center-to-center distance divided by the cylinder diameter, used in the spacing distance effect discussion. The towing speed in this test varies from 0.2 m/s to 1.0 m/s, which corresponds to the reduced velocity range of 2.0-10.0 in the VIV self-oscillation test. To discuss the submergence effect, a non-dimensional depth (h^*) is defined in Fig. 4, $h^*=h/D$, where h is the distance from the lower side of the cylinder to the initial free surface and D is the cylinder diameter. Details of the test cases are shown in Table 1. The submerged depth of the first three cases is set to $h^*=6.8$.

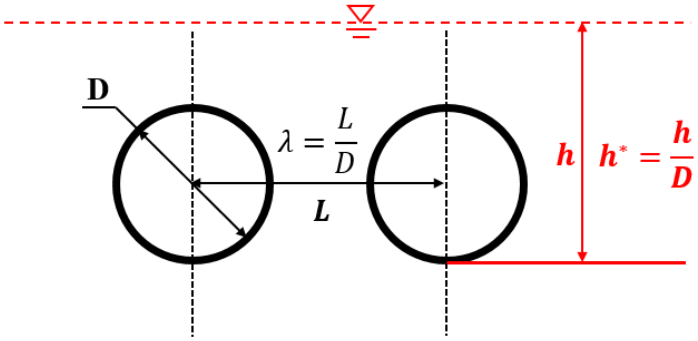

Fig. 4 Sketch of the spacing ratio and submergence concerned in the test

Table 1 Details of the test cases

Case	Spacing ratio	Towing speed (m/s)	Submerged water depth h^*
Validation test (single-cylinder)	-	0.2-1.0	6.8
Stationary model test	2, 3, 4	0.2-1.0	6.8
Self-oscillation test	2, 3, 4	0.2-1.0	6.8
Submerged depth test	4	0.2-1.0	0.1-6.8

3. Basic Theory

The drag forces on the up- (F_{D_U}) and downstream (F_{D_D}) cylinders can be expressed by Eqs. (1) and (2), respectively [6]:

$$F_{D\_U} = \frac{1}{2}\rho C_{D\_U} DlU^2 \quad (1)$$

$$F_{D\_D} = \frac{1}{2}\rho C_{D\_D} DlU^2 \quad (2)$$

where F_{D_U} and F_{D_D} are the mean drag forces on the up- and downstream cylinders in the IL direction, respectively; ρ is the fluid density; C_{D_U} and C_{D_D} denote the mean drag coefficients of the up- and downstream cylinders, respectively; D and l represent the cylinder diameter and length, respectively; and U is the towing speed.

In the discussion of the drag forces and response amplitude properties of the tandem twin cylinders, *Re* and reduced velocity (Ur) [32, 34, 35] are two of the key principal parameters, which can be expressed as follows:

$$\mathrm{Re} = \frac{UD}{\upsilon} \quad (3)$$

$$U_r = \frac{U}{f_n D} \quad (4)$$

where f_n denotes the natural frequency tested in water and υ is the kinematic viscosity coefficient. In this experiment, the ambient temperature is maintained at approximately 15 °C; therefore, υ is approximately $1.14 \times 10^{-6}\, m^2/_s$.

4. Results and Discussion

4.1 Drag Force on a Single Cylinder—Benchmark Test

The drag forces measured in the stationary single-cylinder towing tests are compared with those of the references [36]. Fig. 5 shows a typical time history of the drag force for a stationary single cylinder at a flow velocity of 0.55 *m/s*. The whole drag force history can be divided into five stages: initial (zero force), acceleration, stable, deceleration and final (zero force).

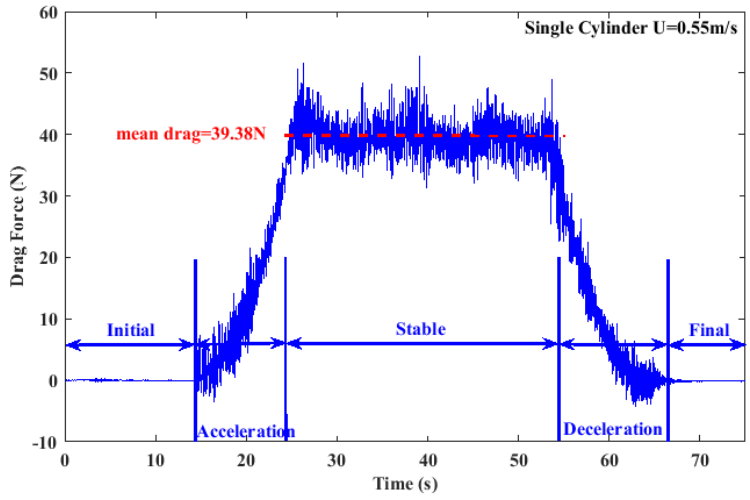

Fig. 5. Time history of measured drag force for a single cylinder

In data processing, the drag force signals are firstly properly treated to maintain a pretty long period of stable. The mean drag coefficient as shown in Fig. 6 can be obtained through Eq. (1). It shows that the experimental results agree very well with the "smooth cylinder" in Achenbach's test [36] .

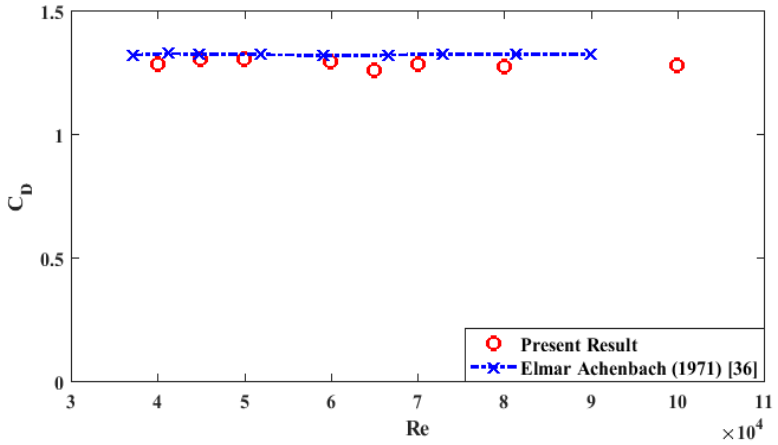

Fig. 6 Mean drag coefficient versus Reynolds number for a single cylinder

4.2 Stationary Model Test of Twin Cylinders

Stationary towing tests of twin cylinders were conducted with three different spacing ratios of 2, 3 and 4; a typical time histories of the drag forces measured from these tests are shown in Fig. 7. The directions of the drag forces on the up- and downstream cylinders are opposite at the cases of λ equals to 2 and 3 where instead of dragging, the force on the downstream cylinder is becoming "driving", and when it comes to $\lambda = 4$ the forces on both cylinders became the same directions . The variations in the wake modes of the upstream cylinder at different spacing ratio have been considered as the main reason for this "driving-dragging" shift. The downstream cylinder is surrounded by low-pressure water in the upstream side formed by the separated shear layers emanating from the upstream cylinder, and its downstream side is surrounded by the water formed by the separated layers emanating from itself. Then, in cases of smaller spacing ratios ($\lambda = 2$ and 3), the pressure from the upstream side is smaller than those from the downstream side of the downstream cylinder, which will lead to "diving" forces on it. When $\lambda = 4$ this will become opposite[37] which might indicate the downstream cylinder is outside of the vortex formation region of the upstream cylinder [7] .

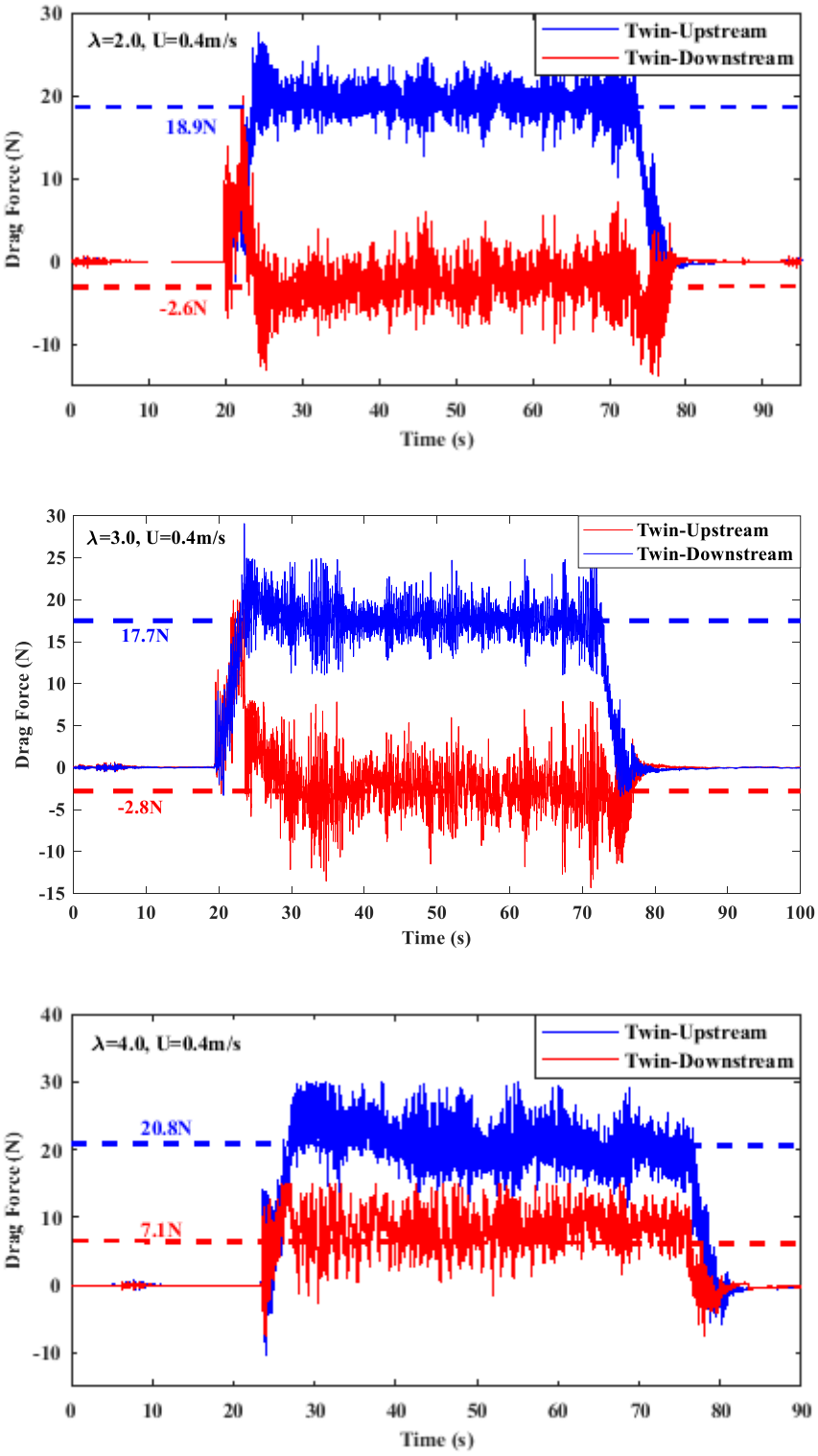

Fig. 7 Time history of drag force for twin cylinders in the stationary model test at a flow velocity of 0.4 *m/s*. The mean drag force shown in the figures are obtained based on the stable stage.

The drag coefficients on the up- and downstream cylinders from the tests are further summarized as in Fig. 8, where the corresponding results on a single cylinder are also provided as references. As shown by the figure, the mean drag coefficient of the

upstream cylinder is larger than that of the downstream cylinder in all the cases due to the shielding effect, as expected. Compared with the single cylinder, the mean drag coefficient of the upstream cylinder is smaller when $\lambda = 2$ and 3, whereas the coefficients are equal when $\lambda = 4$, which means that the effect of the downstream cylinder on the upstream cylinder is diminished when the spacing ratio reaches 4.

In addition, the total and difference of the drag forces on the up- and downstream cylinder are also important for the SFT. The former could be used in the global static analysis of the whole structure, and the latter is the key factor for the connection structure (i.e., the truss system) between the two tubes Eq. (5) further defines the total drag force and the drag force difference.

$$\begin{cases} F_{D\_U} + F_{D\_D} = \dfrac{1}{2}\rho C_{D\_T} D l U^2 \\ F_{D\_U} - F_{D\_D} = \dfrac{1}{2}\rho C_{D\_\delta} D l U^2 \end{cases} \tag{5}$$

where C_{D_T} and C_{D_δ} denote the coefficient of the total drag force and the coefficient of the drag force difference, respectively. As can be seen in Fig. 8, the C_{D_δ} is much larger, even close to that of the single cylinder when $\lambda = 2$ or 3. Meanwhile, the C_{D_T} is much smaller than twice of the coefficient of the single cylinder.

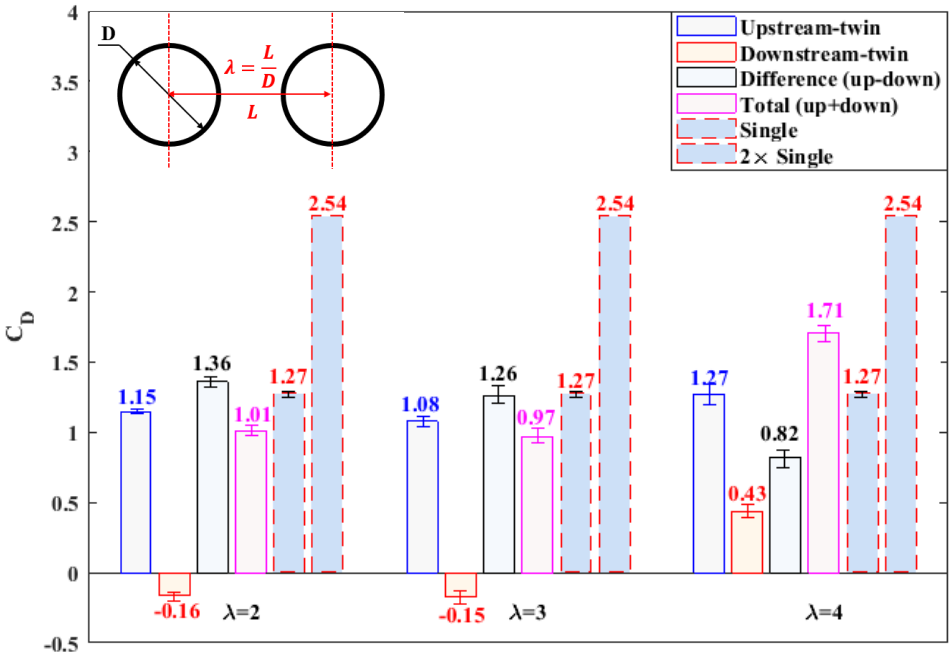

Fig. 8 Mean drag coefficient of a single cylinder and twin cylinders under different spacing ratios (the data displayed the average values of the mean drag coefficient, whereas the ranges on the bars show the mean drag coefficients obtained in the test with different flow velocities).

4.3 VIV Effects on Drag Forces

The current and tide will generate alternatively shedding vortex around the cylinders, which could induce a significant periodical vibration (i.e., VIV), and then cause fatigue damage of the floating tunnel. In addition to conventional periodical CF forces, VIV also will heavily affect the drag forces in IL direction.

Fig. 9 shows the typical time histories of the drag forces on the up- and downstream cylinders under VIV conditions. Similar to the stationary results, the drag forces on the up- and downstream cylinders still act in opposing directions when $\lambda = 2$, but in the same direction when $\lambda = 3.0$ which is different from the stationary tests. That is to say, compared with the stationary testing conditions, VIV changed the pressure distribution around the downstream cylinder. The relative flow direction under VIV conditions is not horizontal anymore, as illustrated by Fig. 10. The angle (α) between the incident flow velocity (U) and the relative flow velocity (U^*) heavily depends on the oscillation velocity ($U_{osc.}$). Therefore, in the lock-in cases (with relatively large response amplitude), the downstream cylinder is no longer immersed in the low-pressure region in the wake of the upstream cylinder, even when $\lambda = 3$. Fig. 11 summarizes the mean drag coefficients of the twin cylinders as a function of reduced velocity, and the drag coefficient of the single cylinder is also presented as a reference.

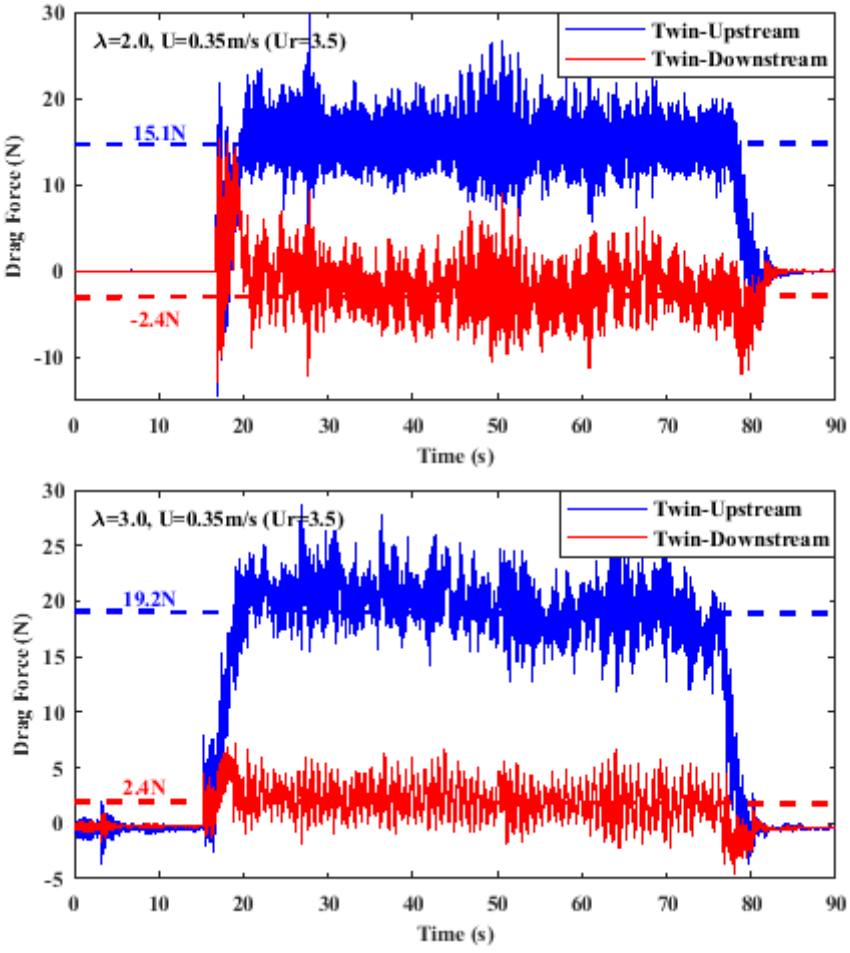

Fig. 9. Time history of drag forces on the up- and downstream cylinders under VIV conditions. The mean drag force shown in the figures are obtained based on the stable stage.

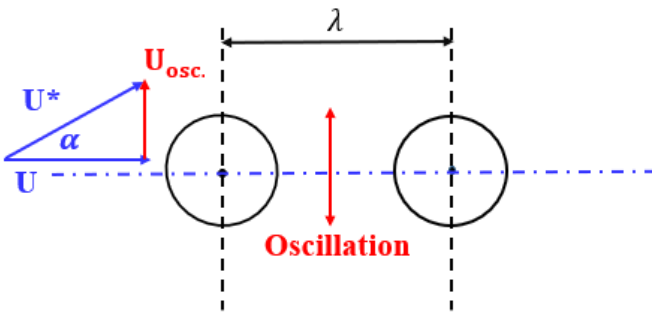

Fig. 10 Sketch of the relative flow velocity in the VIV condition.

Generally speaking, the mean drag coefficients of both cylinders are heavily amplified by VIV compared with the stationary result, namely, the maximum coefficients are increased from 1.27 to 4.1 and 0.43 to 1.7 for up- and downstream cylinder, respectively. The mean drag coefficients of both cylinders are smaller than those of the single cylinder in most cases. The coefficient of the downstream cylinder is even smaller than that of the upstream cylinder because of the shielding effect induced low flow velocity in the gap area.

The drag coefficient of the upstream cylinder strictly follows the trend of the response amplitude with respect to the reduced velocity, whereas the coefficient of downstream cylinder dose not, especially when $\lambda = 4$. In the cases with a small reduced velocity as λ=2 and 3, the mean drag coefficients of both cylinders remain constant. These cases correspond to the zero VIV response amplitude, as shown in Fig. 12. In the following range of reduced velocity, the growth of the response amplitude leads to an increase of the mean drag coefficients on both cylinders except the downstream cylinder when λ=4. When the response amplitude decreases, the drag on the upstream cylinder decreases, whereas the drag on the downstream cylinder remains constant. 'Constant flow mode' in the gap area could be an important reason for the constant drag force on the downstream cylinder if the vortex mode of the upstream cylinder is similar to that of a single cylinder, keeps at '2P' when the amplitude starts to decrease [32] and the constant vortex mode could induce a similar flow mode in the gap area.

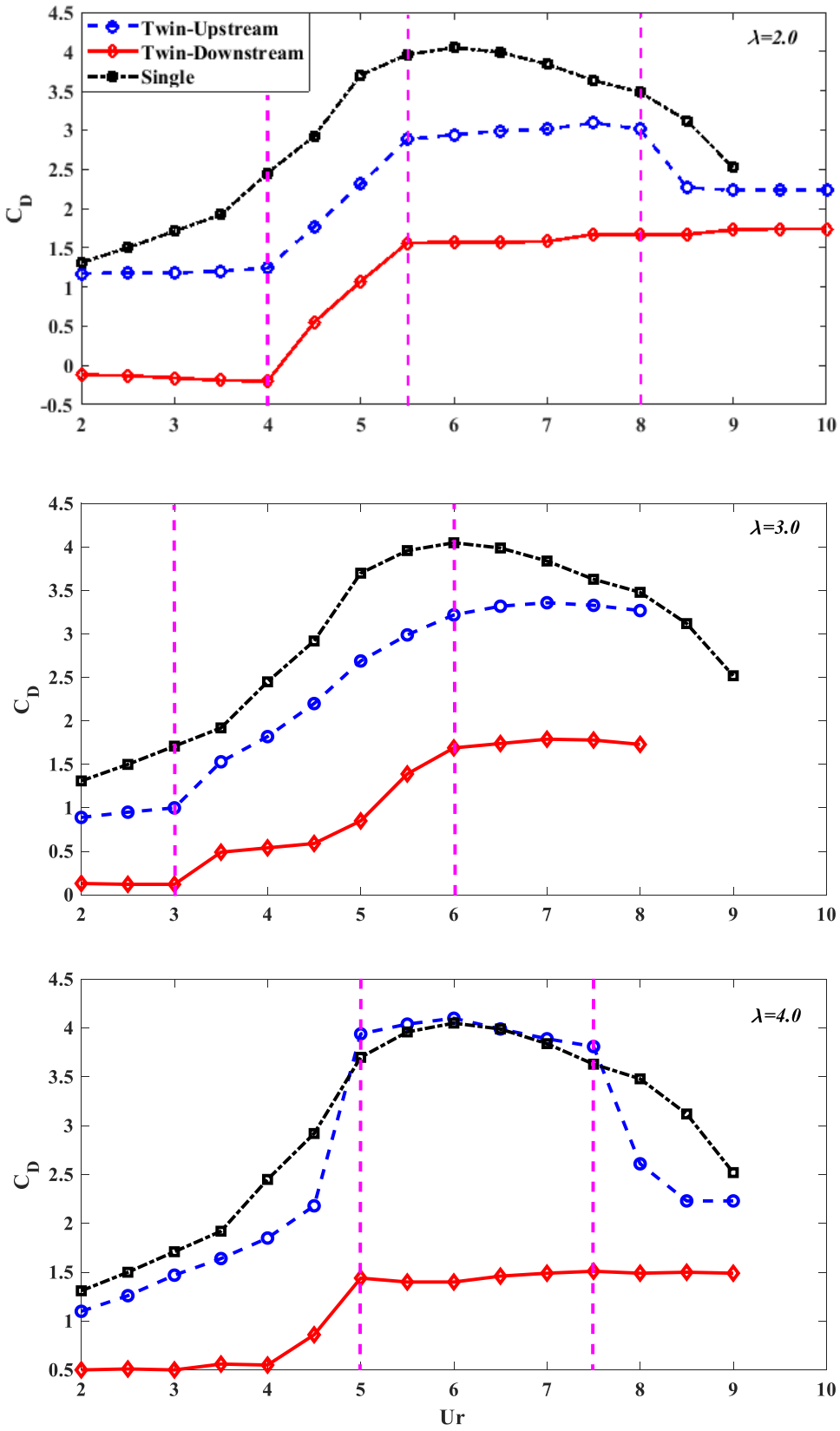

Fig. 11 Mean drag coefficients of the up- and downstream cylinders under spacing ratios of 2, 3 and 4, the values of Ur in this figure also corresponds to the Reynold number dividing 10^4.

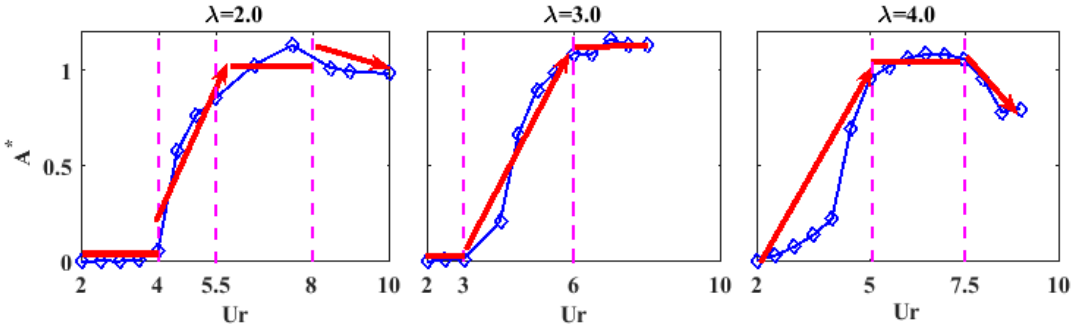

Fig. 12 VIV response amplitude of the twin cylinders for λ =2, 3 and 4 [38]. The blue line shows the response amplitude and the red line shows the main trend ($A^* = A/D$, A is the peak value of response displacement obtained by $rms \times \sqrt{2}$, D is the cylinder diameter).

The VIV amplified mean drag force will determine the largest steady horizontal deformation of the SFT. Therefore, the maximum values of the total drag force and the drag force difference defined in Eq. 5 are studied.

Based on the test results, a novel linear relation is found between the maximum value of the coefficient of the total drag force C_{D_T}, the maximum value of the coefficient of the drag force difference C_{D_δ}, and the spacing ratio λ, as shown in Fig. 13.

$$\begin{cases} C_{D\_T} = (0.1\lambda + 1) * C_D^S \\ C_{D\_\delta} = \dfrac{7}{40}\lambda * C_D^S \end{cases} \tag{6}$$

where C_D^S is the maximum drag coefficient of the single cylinder. If the spacing ratio λ decreases to zero, the total coefficient will be the same as the coefficient of the single cylinder, and the difference will be zero. However, the upper thresholds of these linear relations need further validation in the future. It should be noted here that the three maximum drag coefficients (total, difference and single cylinder) are mostly obtained in the cases of $Ur = 6$. Therefore, these relations could be adopted in the IL loads design of an SFT with a conservative view.

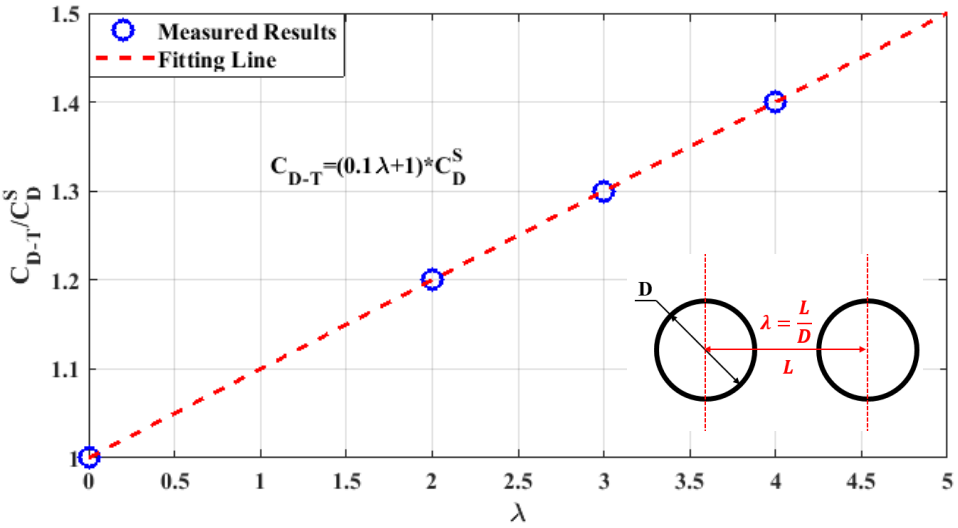

(a) Coefficient of the total drag force

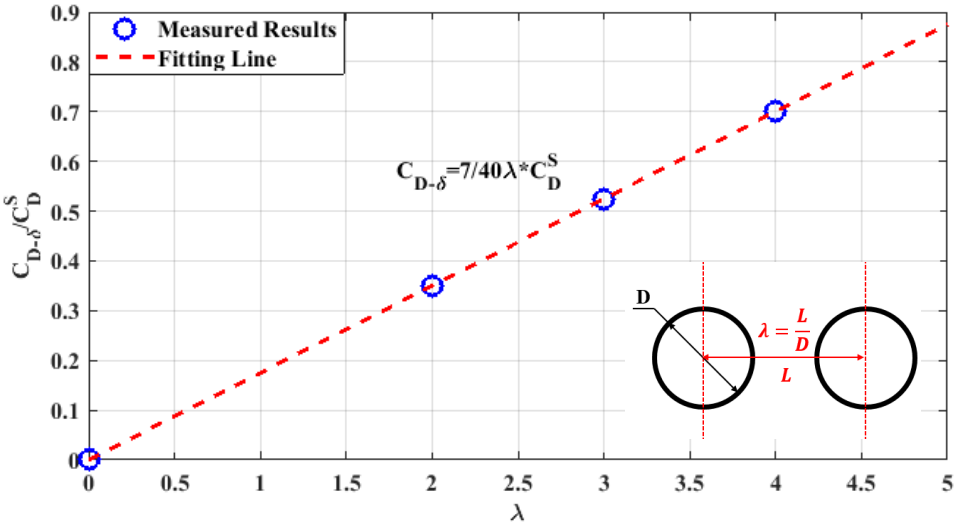

(b) Coefficient of the drag force difference

Fig. 13 Relations between the spacing ratio and C_{D_T} (a), C_{D_δ} (b) with respect to the maximum drag coefficient of the single cylinder $C_D^S = 4$.

4.4 Submerged Depth Effect on Drag

The above results provide a basic reference for the IL load design of the SFT in strong current and tide conditions with a large submergence. In the feasibility design phase shown in Fig. 1, because of the change of the bathymetry, the submergence of the SFT could vary within a range of 24.6 m to 32.6 m [1], and the design of the submerged depth of a SFT should also be a key factor.

Fig. 14 shows the VIV response amplitude of the twin cylinders segment versus the flow velocity under various submergences. It is clearly seen that both factors

significantly affect the VIV response amplitude. Under the first three conditions of $h^* = 6.8, 5.6$ and 3.7, the amplitudes are having very close results, except for the cases when $h^* = 3.7$ while $Ur > 6.5$. It indicates that the response amplitude is irrespective of the submergence when $h^* \geq 5.6$ and $Ur \leq 8$. When $h^* = 2.7$, the amplitudes are similar to those of the former three conditions as $Ur \leq 4.5$ and becomes much smaller as the reduced velocity increases. The amplitude continues to decrease with a decrease in submergence. It can be attributed to the free surface effect, as shown in Fig. 15. The vortex shedding at the upper side near the free-surface is depressed significantly [19]. The weak shear layers lead to a small lift force, which further result in a small oscillation amplitude.

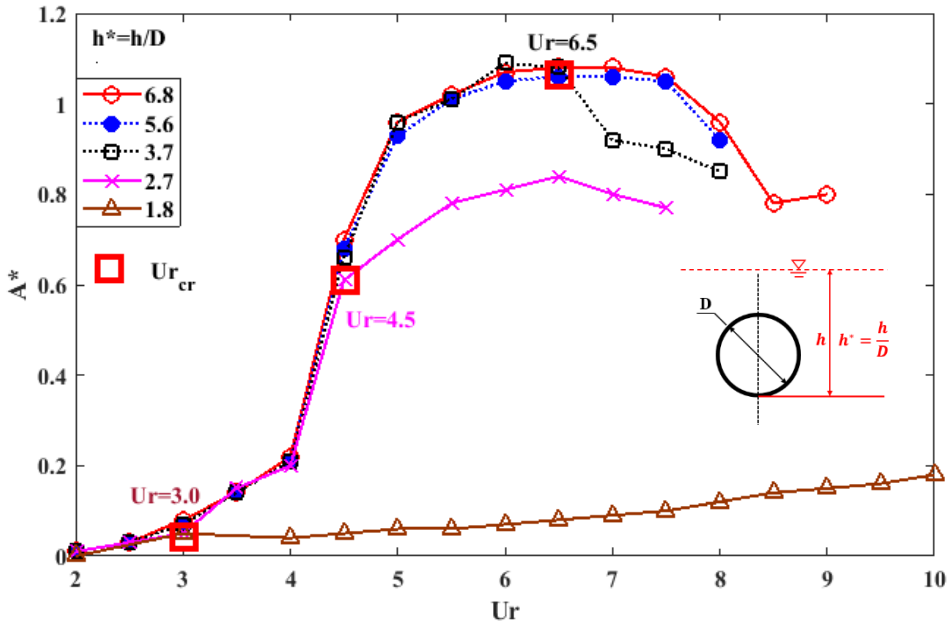

Fig. 14 Response amplitude versus flow velocity under various submergences, the values of Ur in this figure also corresponds to the Reynold number dividing 10^4.

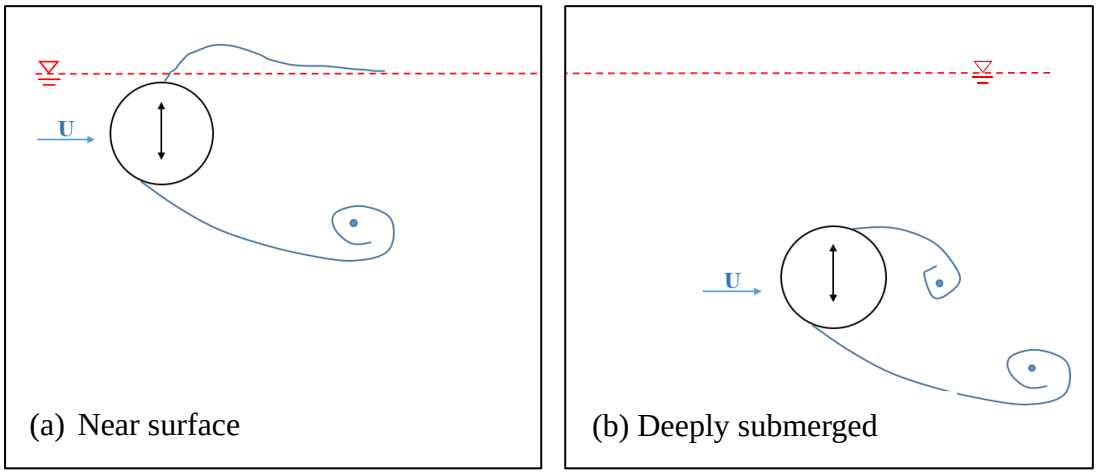

Fig. 15 Configuration of wake patterns for various submergences [6].

In addition to the response amplitude, the mean drag coefficient is also heavily affected by the submergence. Fig. 16 shows the mean drag coefficient of the upstream cylinder under various submergences, which exhibits a similar trend as that of the response amplitude. This mean drag coefficient can reach approximately 4.1 when $Ur = 6$ and $h^* \geq 3.7$. There is a conspicuous decrease in the coefficient when $Ur = 7$ and $h^* = 3.7$. The critical reduced velocity, which is defined by the initiation of the free surface effect, is 4.5 and 3.0 when h^* is 2.7 and 1.8, respectively. When the reduced velocity exceeds the critical value, the free surface effect could lead to a smaller drag coefficient with the decrease of the submergence. In addition, a weak relevance of flow velocity is observed when $h^* = 1.8$. Similar findings were found in the drag coefficient of the downstream cylinder, as shown in Fig. 17.

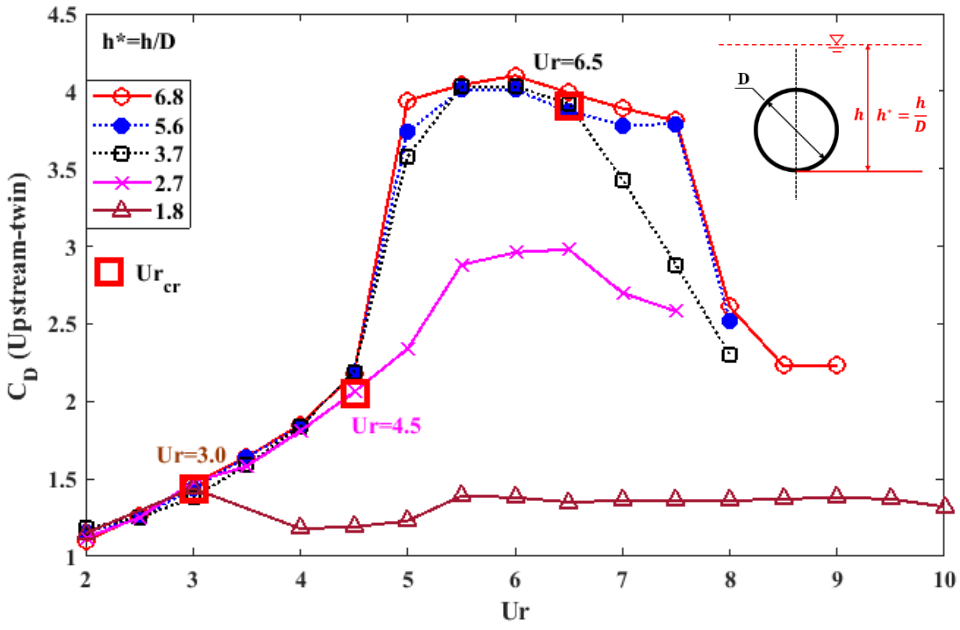

Fig. 16 Mean drag coefficient of the upstream cylinder under various submergences, the values of Ur in this figure also corresponds to the Reynold number dividing 10^4.

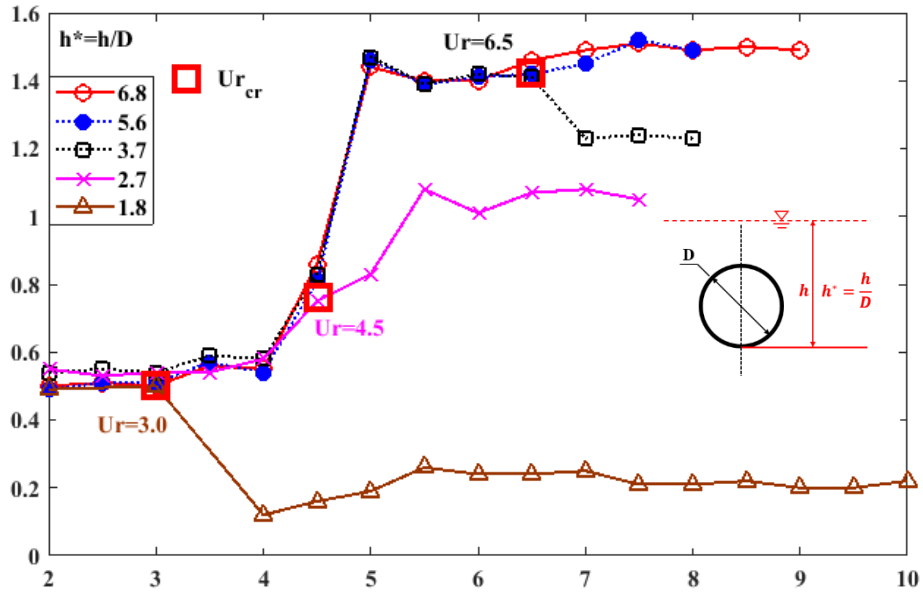

Fig. 17 Mean drag coefficient of the downstream cylinder under various submergences, the values of Ur in this figure also corresponds to the Reynold number dividing 10^4.

The critical value of reduced velocity, $Ur_{cri.}$ heavily depends on the submergence as well as the current velocity, strongly affects the drag coefficient by its influence on the VIV response amplitude. Froude number is usually used to describe the effect of the submergence. However, we did not find a critical case-independent F_r value that can divide the regions whether or not we should consider the free surface effect, as shown in Table 2.

Table 2. F_r number and new defined submerged depth in the test

h^*	Ur_{cr}	$Fr_{cr} = Ur_{cr}\frac{f_n D}{\sqrt{gh}}$
[-]	[-]	[-]
6.8	-	-
5.6	-	-
3.7	6.5	0.34
2.7	4.5	0.28
1.8	3.0	0.23

Therefore, a new principal parameter in terms of flow velocity and submerged depth is introduced to describe the free surface effect on the VIV response amplitude and the drag force for any condition.

In VIV studies of cylinders with large submergence, the reduced velocity ($Ur = \frac{U}{f_n D}$, which is represented in terms of the flow velocity, natural frequency and cylinder diameter) is a widely used key parameter. To illustrate the VIV features that occur in various submergences, a new parameter is defined:

$$h' = \frac{1}{Ur^*} = \frac{hf_n}{U} = \frac{h}{D}\frac{1}{Ur} \qquad (7)$$

where h is the distance between the initial free surface and the lower side of the cylinder. h' is a non-dimensional parameter (or normalized method) and proposed mainly to tell the readers whether or not to consider the free-surface effect at a specific submergence and current velocity. As can be seen in the Eq. 7, the non-dimensional indicator accounts for the effects of submergence, pipe diameter, natural frequency and flow velocity, which are the main parameters that may dominate the free surface effects. The test results further verified the reliability of the implemented approach using this new defined submerged depth.

Fig. 18-20 represent the drag coefficients of the up- and downstream cylinders and the response amplitude versus h'. The dashed lines highlight the critical value of h'. When h'<0.55, the response amplitudes and drag coefficients are smaller than those of the cases with larger submergence at each reduced velocity. However, they are irrespective of the submergence when $h' > h'_{cri.}$. Therefore, the free surface effects must be considered when $h' < 0.55$; and, the hydrodynamic coefficient database obtained from the tests with large submergence is no longer suitable.

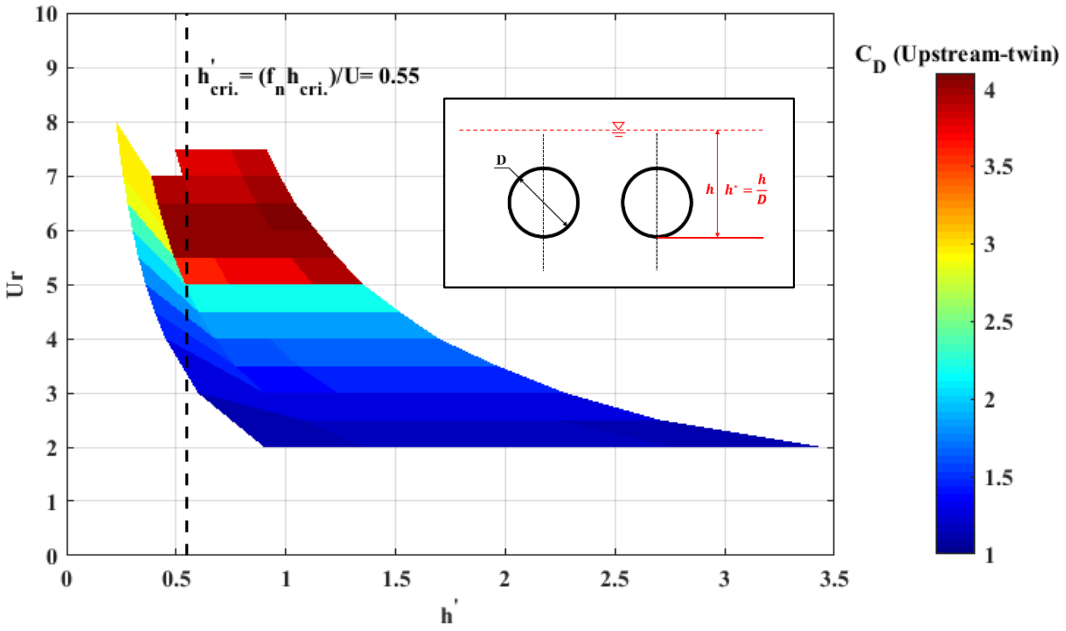

Fig. 18 Mean drag coefficient of the upstream cylinder versus the new defined submerged depth

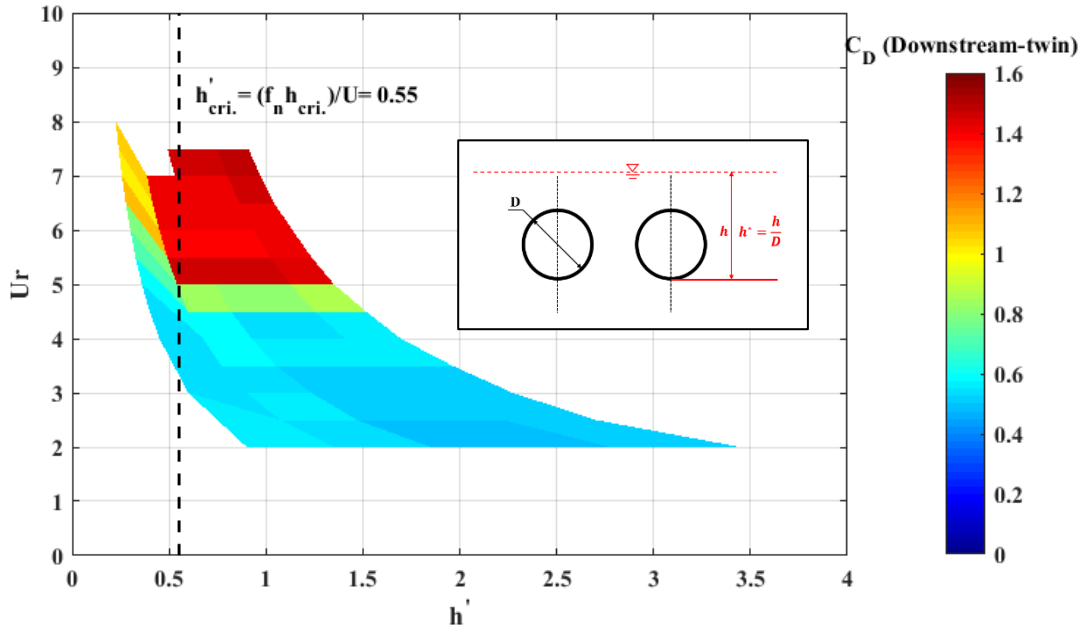

Fig. 19 Mean drag coefficient of the downstream cylinder versus the new defined submerged depth

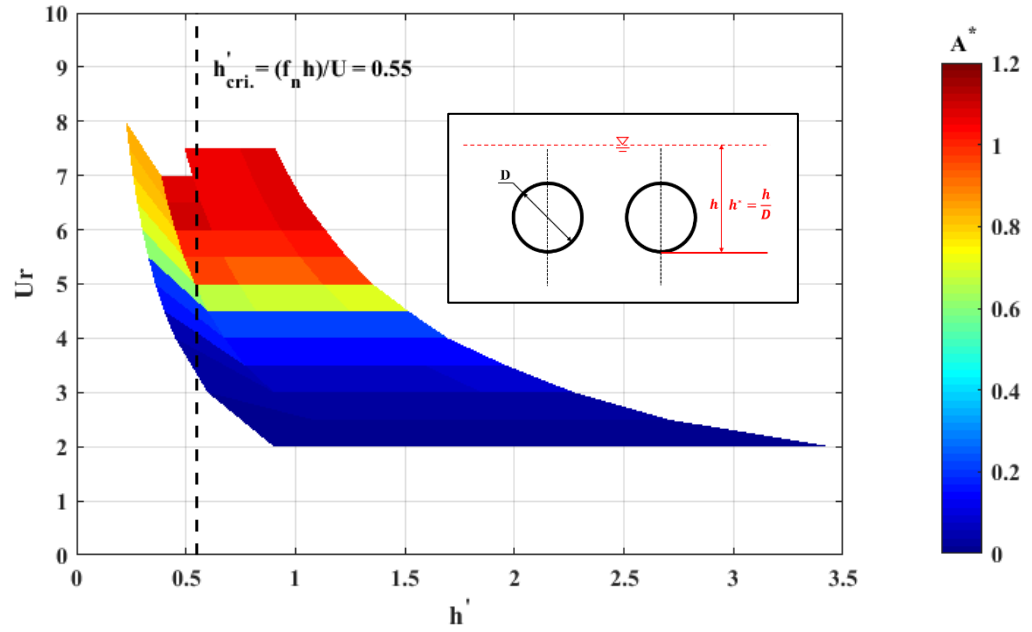

Fig. 20 Response amplitude versus the new defined submerged depth

To provide a simple reference for the floating tunnel design, the maximum value of the coefficient of the total drag force C_{D_T} and the maximum value of the coefficient of the drag force difference C_{D_δ} versus the submerged depth are shown in Fig. 21. In the range of h^* from 1.8 to 3.7, the C_{D_T} and C_{D_δ} are nearly linear with the submerged depth, which is briefly shown in Eq. (8).

$$\begin{cases} C_{D\_T} = (0.5h^* - 1) * C_D^S \\ C_{D\_\delta} = (0.19h^* - 0.05) * C_D^S \end{cases} \quad (8)$$

where C_D^S is the maximum drag coefficient of a deeply submerged single cylinder under VIV conditions.

The above discussion gives a qualitative result of the drag coefficients on twin cylinders with respect to the submerged depth. A new defined nondimensional depth is introduced to describe the free surface effect. However, the testing range of the flow velocity is limited. More cases are suggested to complete the analysis and further validate the present findings, for which the critical is h' 0.55. Particle image velocimetry (PIV) or computational fluid dynamics (CFD) results are also suggested to reveal the mechanics behind the findings presented here.

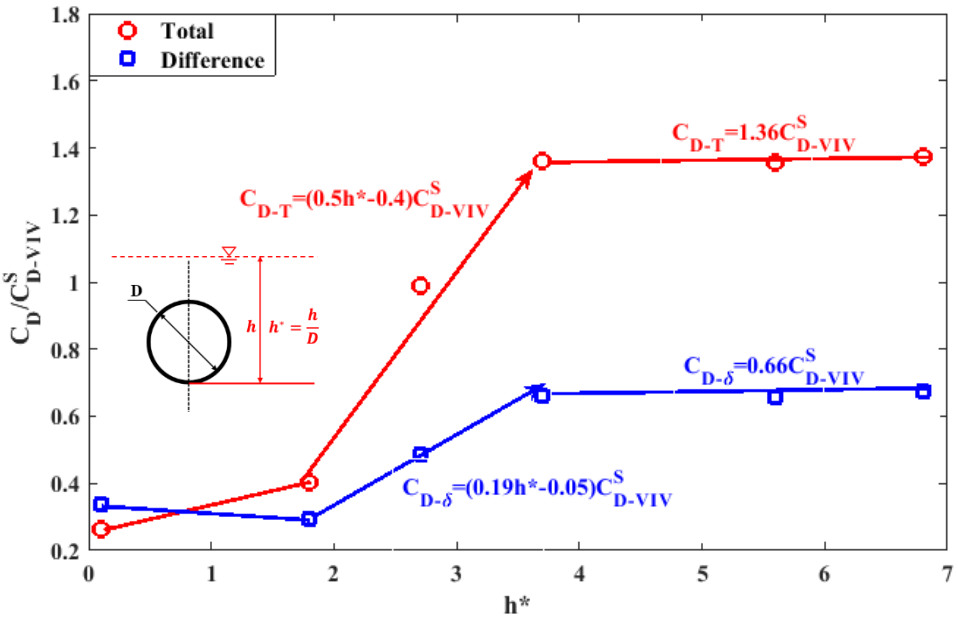

Fig. 21 Maximum value of the coefficient of the total drag force C_{D_T}, maximum value of the coefficient of the drag force difference C_{D_δ} versus the submerged water depth (in terms of the drag coefficient of a deeply submerged single cylinder, $C^S_{D-VIV} = 4$).

5. Conclusions

In this paper, the mean drag forces on rigidly connected tandem twin cylinders are discussed through experiments considering the effects of spacing distance, VIV and submergence. Three spacing distances between the twin cylinders was tested in the experiments, and the VIV-generated drag amplification was discussed within the reduced velocity range of 2.0-10.0. Finally, experiments under different submergences of the model were performed to investigate the free surface effects on the drag forces. The main conclusions drawn from this study are as follows:

(1) In the stationary conditions, the directions of the drag forces on the two cylinders will be opposite when λ =2.0 and 3.0, and the drag coefficient of the upstream cylinder is much larger than that of the downstream cylinder due to the shielding effect. Whereas when λ is equal to or lager than 4, the shielding effects will disappear.
(2) In VIV conditions, both the vibration amplitudes and the spacing ratio heavily affect the drag forces on the twin cylinders. Under smaller spacing ratio, the drag force is nearly 3 times larger than that on the stationary one. Under VIV conditions, a novel feature was revealed namely that the total and difference drag coefficients of the twin cylinder can be described by a linear function of the spacing ratio.
(3) A measure for the submergence when the free surface effect needs to be taken into account is established by introducing a new non-dimensional submerged depth h', the critical value of $h' = 0.55$ is found, namely that, both the VIV response amplitude and the drag forces on the twin cylinders will decrease with decreasing of the submergence when $h' < 0.55$.

Acknowledgments

The authors gratefully acknowledge the financial support by Norwegian Public Roads Administration and supports from the Research Council of Norway through the Centre for Ships and Ocean Structures (CeSOS) and Centre for Autonomous Marine Operations and Systems (AMOS, Project No. 223254) at NTNU. The financial supports from the national Science Fund for Distinguished Young Scholars of China (No. 51825903), Shanghai Science and Technology Program (No. 19XD1402000) are highly acknowledged.

References

[1] Feasibility study for crossing the Sognefjord - Submerged floating tunnel. . Norwegian Public Road Administration (NPRA). 2012. https://www.vegvesen.no/en/Home, download on 1st Feb. 2019.
[2] Vandiver JK. Drag coefficients of long flexible cylinders. Offshore Technology Conference: Offshore Technology Conference; 1983.
[3] Kitagawa T, Ohta H. Numerical investigation on flow around circular cylinders in tandem arrangement at a subcritical Reynolds number. Journal of Fluids and Structures. 2008;24:680-99.
[4] Meneghini JR, Saltara F, Siqueira C, Ferrari Jr J. Numerical simulation of flow interference between two circular cylinders in tandem and side-by-side arrangements. Journal of fluids and structures. 2001;15:327-50.
[5] Schewe G. On the force fluctuations acting on a circular cylinder in crossflow from subcritical up to transcritical Reynolds numbers. Journal of fluid mechanics. 1983;133:265-85.
[6] Sumer BM. Hydrodynamics around cylindrical strucures: World scientific; 2006.

[7] Sumner D. Two circular cylinders in cross-flow: a review. Journal of fluids and structures. 2010;26:849-99.
[8] Chu C-R, Lin Y-A, Wu T-R, Wang C-Y. Hydrodynamic force of a circular cylinder close to the water surface. Computers & Fluids. 2018;171:154-65.
[9] Chung M-H. Two-degree-of-freedom vortex induced vibration of low-mass horizontal circular cylinder near a free surface at low Reynolds number. International Journal of Heat and Fluid Flow. 2016;57:58-78.
[10] Fu S, Xu Y, Hu K, Zhang Y. Experimental investigation on hydrodynamics of floating cylinder in oscillatory and steady flows by forced oscillation test. Marine Structures. 2013;34:41-55.
[11] Ren H, Xu Y, Zhang M, Deng S, Li S, Fu S, et al. Hydrodynamic forces on a partially submerged cylinder at high Reynolds number in a steady flow. Applied Ocean Research. 2019;88:160-9.
[12] Sareen A, Zhao J, Sheridan J, Hourigan K, Thompson M. Vortex-induced vibrations of a sphere close to a free surface. Journal of Fluid Mechanics. 2018;846:1023-58.
[13] Gopalkrishnan R. Vortex-induced forces on oscillating bluff cylinders. WOODS HOLE OCEANOGRAPHIC INSTITUTION MA; 1993.
[14] Jhingran VG. Drag amplification and fatigue damage in vortex-induced vibrations: Massachusetts Institute of Technology; 2008.
[15] Kaiktsis L, Triantafyllou G, Özbas M. Excitation, inertia, and drag forces on a cylinder vibrating transversely to a steady flow. Journal of Fluids and Structures. 2007;23:1-21.
[16] Song L, Fu S, Dai S, Zhang M, Chen Y. Distribution of drag force coefficient along a flexible riser undergoing VIV in sheared flow. Ocean Engineering. 2016;126:1-11.
[17] Khalak A, Williamson C. Fluid forces and dynamics of a hydroelastic structure with very low mass and damping. Journal of Fluids and Structures. 1997;11:973-82.
[18] Khalak A, Williamson C. Motions, forces and mode transitions in vortex-induced vibrations at low mass-damping. Journal of fluids and Structures. 1999;13:813-51.
[19] Bozkaya C, Kocabiyik S, Mironova L, Gubanov O. Streamwise oscillations of a cylinder beneath a free surface: free surface effects on vortex formation modes. Journal of computational and applied mathematics. 2011;235:4780-95.
[20] Reichl P, Hourigan K, Thompson M. Flow past a cylinder close to a free surface. Journal of Fluid Mechanics. 2005;533:269-96.
[21] Sheridan J, Lin J-C, Rockwell D. Flow past a cylinder close to a free surface. Journal of Fluid Mechanics. 1997;330:1-30.
[22] Alam MM, Moriya M, Takai K, Sakamoto H. Fluctuating fluid forces acting on two circular cylinders in a tandem arrangement at a subcritical Reynolds number. Journal of Wind Engineering and Industrial Aerodynamics. 2003;91:139-54.
[23] Carmo B, Meneghini J, Sherwin S. Possible states in the flow around two circular cylinders in tandem with separations in the vicinity of the drag inversion spacing. Physics of Fluids. 2010;22:054101.

[24] Carmo BS, Meneghini JR, Sherwin SJ. Secondary instabilities in the flow around two circular cylinders in tandem. Journal of Fluid Mechanics. 2010;644:395-431.
[25] Alam MM, Sakamoto H, Zhou Y. Determination of flow configurations and fluid forces acting on two staggered circular cylinders of equal diameter in cross-flow. Journal of Fluids and Structures. 2005;21:363-94.
[26] Alam MM, Zhou Y. Phase lag between vortex shedding from two tandem bluff bodies. Journal of Fluids and Structures. 2007;23:339-47.
[27] Borazjani I, Sotiropoulos F. Vortex-induced vibrations of two cylinders in tandem arrangement in the proximity–wake interference region. Journal of fluid mechanics. 2009;621:321-64.
[28] Chen W, Ji C, Williams J, Xu D, Yang L, Cui Y. Vortex-induced vibrations of three tandem cylinders in laminar cross-flow: Vibration response and galloping mechanism. Journal of Fluids and Structures. 2018;78:215-38.
[29] Papaioannou G, Yue D, Triantafyllou M, Karniadakis G. On the effect of spacing on the vortex-induced vibrations of two tandem cylinders. Journal of Fluids and Structures. 2008;24:833-54.
[30] Huang S, Herfjord K. Experimental investigation of the forces and motion responses of two interfering VIV circular cylinders at various tandem and staggered positions. Applied Ocean Research. 2013;43:264-73.
[31] Huang S, Sworn A. Some observations of two interfering VIV circular cylinders of unequal diameters in tandem. Journal of Hydrodynamics. 2011;23:535-43.
[32] Govardhan R, Williamson C. Modes of vortex formation and frequency response of a freely vibrating cylinder. Journal of Fluid Mechanics. 2000;420:85-130.
[33] Song L, Fu S, Cao J, Ma L, Wu J. An investigation into the hydrodynamics of a flexible riser undergoing vortex-induced vibration. Journal of Fluids and Structures. 2016;63:325-50.
[34] Roshko A, Steinolfson A, Chattoorgoon V. Flow forces on a cylinder near a wall or near another cylinder. CALIFORNIA INST OF TECH PASADENA; 1975.
[35] Sheridan J, Lin JC, Rockwell D. Metastable states of a cylinder wake adjacent to a free surface. Physics of Fluids. 1995;7:2099-101.
[36] Achenbach E. Influence of surface roughness on the cross-flow around a circular cylinder. Journal of fluid mechanics. 1971;46:321-35.
[37] Ljungkrona L, Sundén B. Flow visualization and surface pressure measurement on two tubes in an inline arrangement. Experimental thermal and fluid science. 1993;6:15-27.
[38] Deng S, Ren H, Xu Y, Fu S, Moan T, Gao Z. Experimental study of vortex-induced vibration of a twin-tube submerged floating tunnel segment model. Journal of Fluids and Structures. 2020;94:102908.